DOI: 10.17344/acsi.2019.5572 *Acta Chim. Slov.* **2020,** *67,* 570–580

Scientific paper

Adsorption Kinetics for CO_2 Capture using Cerium Oxide Impregnated on Activated Carbon

Azizul Hakim Lahuri,[1,*] Michael Ling Nguang Khai,[2] Afidah Abdul Rahim[2] and Norazzizi Nordin[2]

[1]*Department of Science and Technology, Faculty of Agriculture, Science and Technology, Universiti Putra Malaysia Bintulu Campus, P.O Box 396, Nyabau Road, 97008 Bintulu, Sarawak, Malaysia.*

[2]*School of Chemical Sciences, Universiti Sains Malaysia, 11800 Gelugor, Pulau Pinang, Malaysia.*

** Corresponding author: E-mail: azizulhakim@upm.edu.my*

Received: 09-16-2019

Abstract

Various metal oxides of CeO_2, ZnO, and Co_3O_4 impregnated on activated carbon (AC) were synthesized to determine the CO_2 capture efficiency and analyse with adsorption kinetics model. Batch kinetic studies showed that CeO_2/AC is the most efficient adsorbent with an equilibrium time of 10 minutes that was needed to obtain adsorption capacity of 52.68 mg/g. CO_2 adsorption at 30 °C exhibits the optimum temperature with only 6.53% loss in adsorption capacity after 5 cycles of CO_2 adsorption-desorption. The CeO_2 on AC was detected through X-ray diffraction and the scanning electron microscope image shows well-distributed CeO_2 particles on AC surfaces. CO_2 adsorption at 30 °C is best fitted with the pseudo-second-order kinetics with $R^2 = 0.9994$ and the relative error between calculated and experimental adsorption capacity only 1.32%. The adsorption considering chemisorption is responsible for improving adsorption capacity. The addition of CeO_2 on AC enhanced the adsorption capacity by providing active sites to attract CO_2.

Keywords: CO_2 capture; adsorption kinetics; cerium (IV) oxide; activated carbon; recyclability

1. Introduction

Growing global populations lead to an increasing demand for energy consumption. The same is true for CO_2 gas production resulting from transportation and industrial activities. CO_2 is one of the major greenhouse gases (GHG) that often becomes key environmental concern among policy advocates due to its environmental effects. Based on the National Oceanic and Atmospheric Administration (NOAA),[1] the global CO_2 concentration in the Earth's atmosphere during January 2020 was reported to be 413.40 ppm or which accounts for an increas of 0.63% compared to 410.83 ppm in January 2019. The current annual mean global CO_2 growth rate at approximately 2.94 ppm in 2019 may cause severe climatic change e.g. global warming and rising level of seawater.[2]

In order to reduce the CO_2 emission from a large point source, a process known as Carbon Capture and Storage (CCS) was introduced to fossil fuel power plants.[3] In September 2008, an integrated pilot-scale CCS power plant was commissioned and proven effective to reduce CO_2 emission up to approximately 80% compared to power plants without CCS.[4] In order to sustain a better environment for future generations, several approaches to sorption-based technologies were developed to reduce environmental pollution caused by the massive emission of CO_2 gas.

Amongst the sorption-based technologies developed, adsorption technologies were seen as an alternative to the most mature amine-based solvent processes[5] in the early 1990s.[6] Liquid amine-based absorbent suffers from multiple unfavorable conditions including the corrosive nature of amines, high cost and high regeneration energy.[7] Therefore, the attention has shifted to producing a solid adsorbent which possesses a wider temperature range of regeneration, yields less waste during recycling, and is easier to discard the spent adsorbent.[8] Among these technologies, adsorption-based is preferred over absorption-based due to the drawbacks of absorption with aqueous alkanolamine solutions, such as high equipment corrosion rate, high energy consumption in regeneration and a large requirement for absorbent volume. Adsorbents e.g. amine-based chemical adsorbents with large surface area, large CO_2 adsorption capacity, high adsorption and desorption

rates, high tolerance to moisture, and high selectivity towards CO_2.[9] Furthermore, Yu *et al.* also reported that 60% of total energy is consumed for the regeneration of CO_2-rich chemical absorbents.[9]

CO_2 adsorption on solid sorbents can be classified into two mechanisms namely physical adsorption which involves intermolecular forces and chemical adsorption which involve the sharing of electrons by the adsorbent and the adsorbate.[10] The emerging research in solid CO_2 adsorbents along with their properties and performances provides good insights towards developing the progress in this field. Among the adsorption-based sorbents, it includes the low-temperature solid adsorbents (< 200 °C) such as carbon-based adsorbents,[11] zeolite-based adsorbents,[12] metal-organic framework based adsorbents,[13] alkali metal carbonate-based adsorbents,[14] amine-based solid adsorbents,[15] the intermediate-temperature solid adsorbents (200–400 °C) and high-temperature solid adsorbents (> 400 °C) such as calcium-based adsorbents[16] and alkali ceramic-based adsorbents.[7] Hence, a further modification to obtain easy handling in comparison to liquid absorbent by using support materials to impregnate the amine-based sorbent is being sought. Several amine-based adsorbents were reported such as monoethanolamine (MEA) on activated carbon (AC) that exhibit low adsorption capacity (15.40 mg/g) due to the large molecule coating the AC microporous surfaces.[17] Kamarudin *et al.*[18] reported various types of amine-functionalized kenaf with tetraethylenepentamine (TEPA), which showed higher adsorption capacity (40.22 mg/g) than MEA on kenaf and raw kenaf. A larger molecule of octadecylamine (ODA) on silica gel (SG) pre-treated at 600 °C was found to have similarly adsorption capacity (15.61 mg/g)[15] as MEA on AC.

The calcium-based adsorbent is a classically used metal oxide adsorbent for capturing CO_2 due to its high reactivity with CO_2 and low-cost material. The reversible reaction between CaO and CO_2 is shown in Equation 1. The forward reaction shows the adsorption of CO_2 at a temperature between 600 to 700 °C[7] to form $CaCO_3$ while backward reaction depicts the regeneration of CO_2 but requires high heat supply between 900 and 950 °C for the next cycle of CO_2 adsorption.[19–21]

$$CaO\ (s) + CO_2\ (g) \rightleftarrows CaCO_3 \quad (1)$$

Therefore, an alternative metal oxide was used as adsorbent of CO_2 e.g. iron oxides (FeO, Fe_2O_3, and Fe_3O_4),[22] TiO_2,[23] γ-Al_2O_3,[23] CeO_2,[24] SiO_2,[24] ZrO_2,[24] and ZnO.[25] According to Chanapattharapol *et al.*,[10] iron oxide doped MCM-41 adsorbent prepared by impregnation reported higher CO_2 adsorption than the undoped MCM-41 partly due to increased surface area and electron transfer from metal to CO_2. Numerous studies were reported on the CO_2 adsorption on AC due to its wide availability, low cost, and green production. However, AC only offers a weak interaction by physisorption.[22] Thus, surface modification on the carbonaceous support can contribute to higher selectivity towards CO_2 and increase the adsorption capacity of the porous material. AC surface modification by adding metal oxide of alkali metal, alkaline earth metal, and transition metal provides basicity sites on the AC surfaces. A study reported a successful surface modification of AC loaded with Fe_2O_3 with 103.7 mg/g adsorbent with physisorption mainly contributed by AC and chemisorption contributed by Fe_2O_3.[26] Other studies reported using NiO,[27] MgO[28] and CuO[29] to modify the AC surfaces and enhance its adsorption capacity. It is notable to highlight that metal oxide load-

Table 1. Adsorption capacities of various adsorbents.

Adsorbent	Adsorption Capacity (mg/g)	Adsorption Temperature (°C)	CO_2 Purity	Sources
35%ODA/SG600	15.61	25	99%	15
MEA/AC	15.40	25	15%	16
Raw kenaf	27.46	30	99.99%	17
50%MEA-Kenaf	34.36	30	99.99%	17
50%TEPA-Kenaf	40.22	30	99.99%	17
MCM-41	35.00	25	n.a	10
Fe_2O_3/MCM-41	38.40	25	n.a	10
NiO	14.14	25	99%	25
CeO_2	48.00	25	≥ 99.5%	30
Fe_2O_3	17.00	25	99%	31
SiO_2	33.73	25	99%	32
1%[bmim][CF_3SO_3]/SiO_2	66.71	25	99%	32
10%NiO/[emim][HSO_4]/SiO_2	48.80	25	99%	33
10%[emim][HSO_4]/SiO_2	26.70	25	99%	33
10%ChCl:U/SG200	22.30	30	99%	34
ChCl:U/AC	39.40	25	15% in N_2	35

n.a is not available

ing on AC increases the adsorption capacity because it attracts significantly more CO_2 to be chemically bonded and provide better chemisorption properties for the adsorbent.

Recently, ionic liquid-based and deep eutectic solvent (DES)-based materials were applied to the CO_2 capture. Marliza *et al.* reported that ionic liquid functionalized SiO_2 shows highest adsorption capacity for 1-butyl-3-methylimidazolium trifluoromethanesulfonate, [bmim][CF_3SO_3]/SiO_2 than SiO_2 alone.[32] Addition of NiO to the 1-ethyl-3-methylimidazolium hydrogensulfate, [emim][HSO_4] functionalized SiO_2 shows enhanced adsorption capacity due to higher surface area than 10%[emim][HSO_4]/SiO_2.[33] Green technology application through the DES of Choline chloride: urea (ChCl:U) is biocompatible, non-toxic, biodegradable, inexpensive and easy to prepare.[34] The ChCl:U functionalized silica gel was found to have lower adsorption capacity (22.30 mg/g) due to lower surface area (317.50 m^2/g)[34] of the adsorbent rather than ChCl:U functionalized AC,[35] which exhibits higher surface area (581.23 m^2/g) and adsorption capacity. Nonetheless, the significance of desorption properties for the adsorbents are not reported for these works. The performance of various adsorbents is reported in Table 1.

In the present work, double activation will be performed on AC to reactivate the surfaces. The metal oxides of ZnO, CeO_2, and Co_3O_4 were added to the modified AC. These metal oxides were chosen based on the previous study which the metal oxides on AC are not yet discovered its adsorption capacity and adsorption kinetics. Hence, the specific aim of this work is to measure the adsorption capacity, evaluate the desorption properties, identify the most efficient metal loaded on AC, and determine optimum adsorption temperature with adsorption kinetics analysis for CO_2 capture.

2. Experimental

2. 1. Sample Preparation

Charcoal activated carbon (Qrec), cobalt (II) sulfate heptahydrate (Hamburg), cerium (III) nitrate hexahydrate (Nacalai Tesque), and zinc sulfate heptahydrate (R&M) were used as precursors. Moisture removal was conducted by drying the AC in an oven for 2 hours at 110 °C. Double activation of AC was performed by using readily purchased AC to reactivate by using $KMnO_4$. For the support treatment, AC was weighed to 5 g and was added into a solution of 0.1 M $KMnO_4$. The mixture was shaken for 20 minutes at 200 rpm and followed by filtering and rinsing with 200 mL distilled water. The AC was dried in an oven overnight at 110 °C. The adsorbents were prepared by a conventional wet impregnation method. Generally, 0.1 M metal salt was prepared in a 50 mL volumetric flask. AC was subsequently added into the metal salt solution and shaken for 8 hours at 200 rpm. The mixture was filtered and rinsed with 400 mL of 1% $NaHCO_3$ solution, followed by soaking overnight in 600 mL of 1% $NaHCO_3$ solution. Soaked samples were filtered and rinsed with distilled water and allowed to air dry for 2 hours. The samples were dried overnight in an oven at 110 °C. The resultant adsorbents were denoted as metal oxide/activated carbon (MO/AC) where MO represents Co_3O_4, CeO_2, ZnO.

2. 2. CO_2 Adsorption and Desorption

The CO_2 adsorption was measured by using thermogravimetric analysis-derivative thermogravimetry (TGA-DTG) from a Simultaneous Thermal Analyzer (STA) 6000, Perkin Elmer. Approximately 10 mg of each sample was cleaned at 350 °C in the N_2 atmosphere prior to adsorption measurement. The adsorbent was heated from 30 to 350 °C at 30 °C/min and was cooled to 30 °C. The CO_2 adsorption was conducted at 30 °C for 20 minutes. Then, the adsorption capacity was measured from the weight gained after the saturation exposure. Finally, the gas feed was switched to the N_2 atmosphere and was heated again up to 900 °C for the desorption process. The carbonate dissociation temperature was determined to perform the recyclability test at different adsorption temperature.

2. 3. Adsorbent Characterization

The infrared spectra of various metal oxides supported on AC were recorded between 400 and 4000 cm^{-1} using FTIR (PerkinElmer) with KBr pellet method for sample preparation. N_2 adsorption-desorption isotherms were measured on a static volumetric technique instrument (Micromeritics ASAP 2020) for determination of the Brunauer-Emmett-Teller (BET) surface area, mesopore surface area, micropore surface area, total pore volume, micropore volume, and the average pore diameter. The pore size distribution was computed using density functional theory (DFT) method. Approximately 0.5 g of each adsorbent was degassed at 350 °C under vacuum prior to the measurement for the elimination of humidity gases trapped in the adsorbents. In this regard, a water circulating bath was used to control the temperature. The N_2 adsorption-desorption isotherms were recorded at liquid nitrogen temperature of 77 K, and applied in a relative pressure (P/Po) ranging from 0 to 1.0. The surface area (S_{BET}) was calculated by using a commonly used method called Brunauer-Emmett-Teller (BET) method. All surface area measurements were calculated from the nitrogen adsorption-desorption isotherms by assuming the N_2 molecule to be 0.162 nm^2. The t-plot method was used to calculate the mesopore surface area (S_{meso}), micropore surface area (S_{micro}) and micropore volume (V_{micro}). The total pore volume (V_{tot}) was obtained by converting the amount of N_2 gas adsorbed (in cm^3/g at STP) at relative pressure to the volume of gas adsorbate.

The most efficient adsorbent was characterized by its phase composition and surface morphology. X-ray Dif-

fraction (XRD) pattern was obtained by using XRD diffractometer (Bruker D8 Advance). The crystal structures were verified by recording 2θ diffraction angle from 10° to 70° and matched with the standard diffraction data (JCPDS) file for interpretation of the crystalline phase. The surface micrograph of the most efficient adsorbent was observed using a scanning electron microscope (SEM, Quanta 650 field emission gun).

2. 4. Adsorption Optimization and Recyclability Test

The most efficient adsorbent was optimized with different adsorption temperatures of 30 and 50 °C. The recyclability test was performed for 5 cycles of CO_2 adsorption and desorption by using the aforementioned TGA-DTG analysis. Generally, for the first cycle, the adsorbent will start with the cleaning process, cooled to desirable adsorption temperature (30 or 50 °C), CO_2 adsorption, and CO_2 desorption process. After cooling to the desirable adsorption temperature, the second cycle CO_2 adsorption starts again and followed by the desorption process. These methods were repeated up to 5 times to determine the regeneration properties of selected adsorbents.

2. 5. Adsorption Kinetics Study

The experimental data for CO_2 adsorption of the most efficient adsorbent at different adsorption temperatures were analyzed with kinetic models such as the pseudo-first-order kinetic model and pseudo-second-order kinetic model. The adsorption kinetics describes CO_2 uptake rate controls with adsorption time of adsorbate uptake at the solid and gas interface.

3. Results and Discussion

3. 1. Adsorbent Characterization

FTIR spectra were recorded to investigate the functional groups of activated carbon before and after impregnation with various metal oxides as it offers the properties of molecules and characteristics of chemical bonds. The IR spectra and absorption bands are shown in Figure 1 and Table 2, respectively. A typical band at 3406 cm^{-1} is indicative of O-H stretching due to the hydrogen bond caused by moisture content in the sample.[22] The intensity of the strong band decreased after impregnating the metal oxide onto the activated carbon. The decrease in the moisture content was due to the metal oxides deposited on the AC, thus, trapped the the moisture.

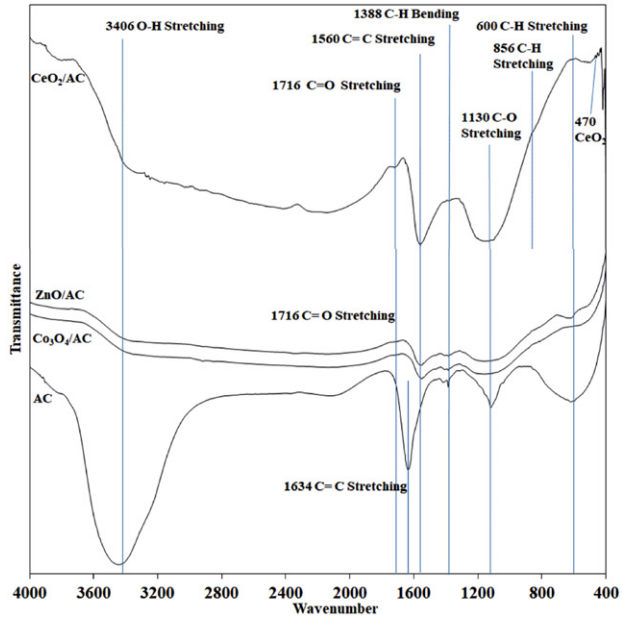

Figure 1. IR spectra of AC and various MO/AC.

Table 2. Vibrational frequencies IR spectroscopy of various MO/AC.

Vibrational modes	This study (cm^{-1})	Reference (cm^{-1})
O-H Stretching	3406	3412
C=O stretching	1716	1716
C=C Stretching	1634	1633
C=C Stretching	1560	1550
C-H Bending	1388	1390
C-O Stretching	1130	1130
C-H Stretching	600	600
Ce-O	470	459

The bands at 1643, 1388 and 600 cm^{-1} are reported to be characteristic absorption bands of activated carbon corresponding to C=C stretching, C-H bending and C-H stretching, respectively.[36] The decrease of intensities in these bands after impregnation with metal oxides indicates that the deposition of metal oxides has reduced the absorption bands for AC.[37] Nonetheless, reactivating the AC for the MO/AC adsorbents contribute to the alteration of surface nature by introducing oxygen-containing functional groups of C=O at 1716 $cm^{-1}$and changing intensities for C-O stretching at 1130 cm^{-1}. This explains $KMnO_4$ oxidizing the surface of AC, besides forming pores structure, which is in agreement with Zhang *et al.*[38] The peak at 1634 cm^{-1} shows a large redshift of 74 cm^{-1} compared to 1560 cm^{-1}, after loading of metal oxides which also occurred when using silver loaded on activated carbon by Zhao *et al.*[39]. In addition, the bands at 470 cm^{-1} are ascribed to the characteristic bands of metal oxides CeO_2,[40] respectively.

The N_2 adsorption-desorption isotherms are shown in Figure 2. According to the International Union of Pure and Applied Chemistry (IUPAC) classification, all of the isotherms exhibit Type I isotherm.[41] The initial steep region is attributed to strong adsorption by a typical microporous material. Hysteresis loop closing at around relative pressure of 0.4 can be observed in all isotherms, indicating

Table 3. The textural characteristics of the adsorbents.

Adsorbent		AC	CeO_2/AC	ZnO/AC	Co_3O_4 /AC
Surface area	S_{BET} (m^2/g)	1043.6	763.4	792.9	838.5
	S_{meso} (m^2/g)	171.0	254.1	280.4	302.2
	S_{micro} (m^2/g)	872.6	509.4	512.5	536.3
Pore Volume	V_{total} (cm^3/g)	0.46	0.42	0.45	0.47
	V_{micro} (cm^3/g)	0.35	0.21	0.21	0.22
Average pore diameter (nm)		1.8	2.2	2.3	2.2

S_{BET} is surface area by BET method; S_{mic} is the micropore surface area by t-plot method; V_{total} is single point total pore volume; V_{micro} is micropore volume obtained by the t-plot method

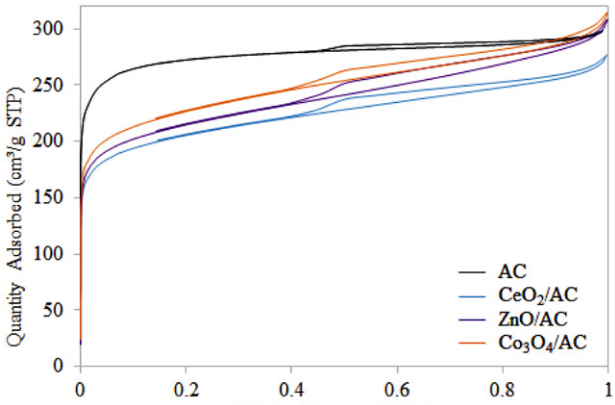

Figure 2. N_2 adsorption-desorption isotherms of the adsorbents.

that the mesoporosity of slit-shaped pores is present in the samples.[26] The adsorbents show H4 hysteresis which is associated with porous materials and indicates a narrow slit-shaped pore.[42] The N_2 adsorption-desorption isotherm for AC has the highest steep initial region ascribed from high micropore structure that easily occupied. The hysteresis of metal oxides loaded AC shows a larger area indicating of high mesopore structure. These are correlated with the textural properties as indicated in Table 3. The formation of mesopores may be explained by the metal oxide burning off carbon wall and enlarging pore sizes during thermal treatment.

The BET surface area decreased with the loading of metal oxides onto AC samples (Table 3). This also suggests that the pores of the AC are blocked or covered.[26] However, an increase in micropore surface area and mesopore surface area ascribed to reactivation of ACs by chemical treatment with $KMnO_4$ prior to metal oxide impregnation. It is notable that Co_3O_4/AC has a higher surface area compared to CeO_2/AC and ZnO/AC. We presume that the Co_3O_4 particles are deposited on AC surfaces instead of pores due to larger particle size. Thus, the pores generated from Co_3O_4 also contribute to the increment of the adsorbent's surface area. The reduction in micropore volume after impregnation with metal oxides is mainly attributed to the addition of metal oxides particles which tend to deposit on the AC surface. In other words, the deposited metal oxides particles fill in the pores of AC surface.

Next, the DFT method was used to compute pore size distribution (Figure 3) of the microporous AC containing various metal oxides. Although AC has a lower intensity of distribution at the region of 9–12 Å (0.9–1.2 nm) as shown in the inset of Figure 3, the AC possessed the highest pore distribution in the region of 16–20 Å (1.6–2.0 nm). Thus, it has a high distribution of micropore structure in which the diameter of the pores is below 2 nm. Most of the metal oxides generated are unable to enter the pores below 12 Å (1.2 nm) because the distribution in the region is less affected. Nonetheless, the distribution in the region of 16-20 Å (1.6–2.0 nm) was diminished, possibly be due to the fine particle metal oxides capable to enter the AC pores, or deposited on the AC pores. Above 21 Å (2.1 nm), higher pore size distribution compared to AC alone attributed by the pores generated from metal oxides themselves.

Thermal stability of various metal oxides impregnated on AC was later computed using the TGA-DTG by heating up to 900 °C (Figure 4). The initial steep region of weight loss was explained by moisture removal. No distinct peak of derivative weight loss was observed at higher

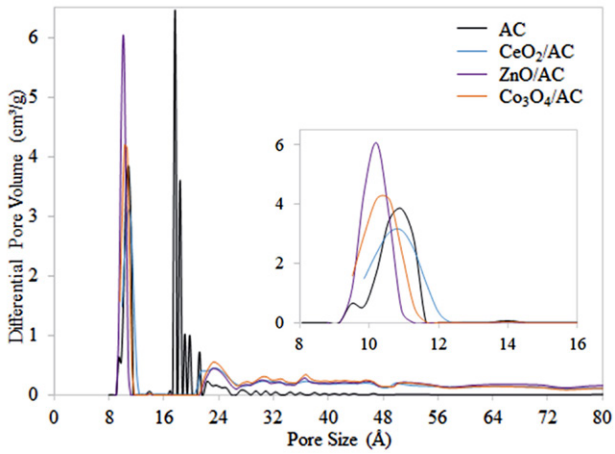

Figure 3. Pore size distribution with the inset image shows clearer pore size distribution at the range of 8-12 Å (0.8–1.2 nm).

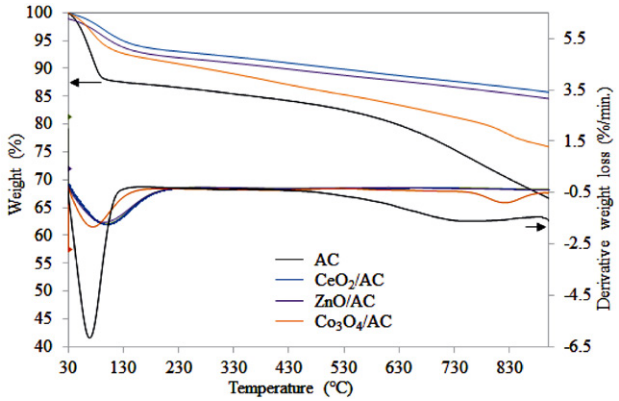

Figure 4. Thermal stability of the adsorbents.

temperature. This implies the samples were resistant to heat. The Co_3O_4/AC shows a derivative weight loss peak at a temperature of 830 °C which corresponded to the decomposing temperature of Co_3O_4.[43]

3. 2. CO_2 Capture

CO_2 capture was performed using TGA and the wide-angle of the thermograms was plotted as shown in Figure 5. The CO_2 adsorption and desorption processes which equalize to its origin were plotted as depicted in Figures 6a and 6b, respectively. The adsorption capacity was obtained from the weight gain shown in Figure 6a. At the beginning of the adsorption, it is observed that the initial steep increase indicates the amount of CO_2 adsorbed on CeO_2/AC and AC is faster than ZnO/AC and Co_3O_4/AC. Eventually, the adsorption gradually decreases when the progress of the adsorption process reaches equilibrium. Figure 6a demonstrates that the adsorption process has reached equilibrium state at the time of 5 minutes for AC and Co_3O_4/AC; 10 minutes for CeO_2/AC; 13 minutes for ZnO/AC. Steep initial region corresponds to stronger binding force between CO_2 with metal oxides and CO_2 with micropores of AC. At the knee-shaped region, the multilayer CO_2 adsorption on the adsorbent formed by occupying CO_2 adsorbate on the uneven bonded CO_2 surface and creating CO_2-CO_2 interaction. It is noteworthy to observe that CeO_2/AC and ZnO/AC show higher adsorption capacity at equilibrium state compared to AC only. This is indicative of CeO_2 and ZnO to possess higher basic properties compared to Co_3O_4. Whereas AC was unable to hold CO_2 strongly compared to those with the presence of metal oxides on AC. Although AC only exhibits the highest surface area, the adsorption capacity was observed to be lower than with CeO_2/AC. Reactivating the AC by using chemical activation of $KMnO_4$ may improve AC surface nature, changing the properties of AC, including pore structure and purity. The significance of double activation increasing the oxygen functional group results in enhancement of AC surfaces and adsorption capacity.

Furthermore, the AC surface modification by impregnation of CeO_2 provides basic active sites that are mainly responsible for the formation of carbonate species and enhancing adsorption capacity. The formation of carbonate species by CO_2 chemisorption reaction pathway can be simplified as in Equation 2.

$$CO_2\ (\text{adsorbate}) + O\ (\text{surface of } CeO_2) \rightarrow \rightarrow [CO_2\text{-}O] \rightarrow CO_3\ (\text{chemisorption}) \quad (2)$$

The chemisorption allows the active sites from the oxygen surface of CeO_2 to exchange electron with CO_2 forming carbonate species product. This could be the reason for the presence of metal oxides that may hold the CO_2 firmly at equilibrium state compared to AC only. Lower in adsorption capacity for Co_3O_4/AC compared to AC only might also be attributed to the weakly adsorbed CO species by cobalt ion which can be fully desorbed at 230K (–43 °C) as reported by Ferstl *et al.*[44]

The thermograms for the desorption process (Figure 6b) shows CeO_2/AC has the highest weight loss up to around 400 °C for CO_2 regeneration. It has a relatively lower CO_2 desorption temperature of 160-280 °C.[45] Hence, the carbonate product will be dissociated to regenerate as CO_2 and leaving the adsorbent that is suitably reused for the next cycle. The desorption temperature above 400 °C resulting in greater weight loss for all adsorbents. Thus, the desorption temperature up to 400 °C will be deployed for the recyclability test.

The adsorption capacity for all adsorbents and similar works are tabulated in Table 4. Among the synthesized adsorbents, CeO_2/AC shows the highest adsorption capacity of 52.78 mg/g at equilibrium. Therefore, CeO_2/AC was chosen as the most efficient adsorbent for further performance optimization through the recyclability test at different adsorption temperature. In comparison, the unmodified AC, which was used to load with 10% CeO_2 (ACCe-HT) and CuO (ACCu-HT) separately by using hydrothermal treatment,[46] shows lower adsorption capacity than this work (Table 4). Meanwhile, Heo *et al.*[28] deployed a slightly complicated method than the one of this work but obtained a comparable CO_2 adsorption capacity through 12 minutes microwave radiated synthesis of MgO on microporous carbon (MC).

Several common activating agents were reported such as zinc chloride ($ZnCl_2$), potassium hydroxide (KOH), hydrochloric acid (HCl), nitric acid (HNO_3) and phosphoric acid (H_3PO_4).[47] This study reported double activation of AC by reactivating with $KMnO_4$. The significance of chemical activation over physical activation was reported in which chemical activation by using $ZnCl_2$ is a promising method to obtain better textural properties for AC derived from palm kernel shell (PCAC).[48] By loading BaO on PCAC, it was observed to be the best adsorbent for CO_2 capture ascribed from the highest BET surface area. Meanwhile, Plaza *et al.*[49] reported AC from the

Table 4. Adsorption capacities of various sorbents.

Adsorbent	Adsorption Capacity (mg/g)	Adsorption Temperature (°C)	CO_2 Purity	Sources
AC	52.01	30	99%	This study
CeO_2/AC	52.78	30	99%	This study
ZnO/AC	52.06	30	99%	This study
Co_3O_4/AC	43.17	30	99%	This study
ACCe-HT	37.66	30	20%	47
ACCu-HT	25.74	30	20%	47
Mg-MCs-12	53.68	40	15% in N_2	28

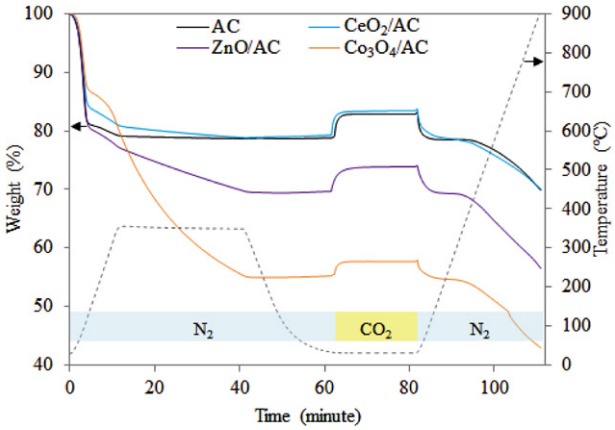

Figure 5. Simultaneous CO_2 adsorption and desorption for all adsorbents with adsorption temperature of 30 °C.

spent coffee ground to show higher CO_2 adsorption capacity by chemical activation using KOH than physical activation.

The phase composition of CeO_2/AC was determined by XRD diffractograms as shown in Figure 7. Typical graphitic structure for AC with broad amorphous diffraction peaks at 2θ values of 26° and 43°. After loading with CeO_2, the amorphous peaks decreased and shifted from 26° and 43° toward 29° and 48° respectively. Another new diffraction peak was observed at 56°. These three diffraction peaks are the reflections of the (111), (220) and (311) crystallographic planes of the cubic CeO_2 phase.[50] The CeO_2/AC surface morphology (Figure 8) shows the well-distributed of fine particles CeO_2 on AC surfaces. Reactivating the AC results in scavenging effect to the AC surface and

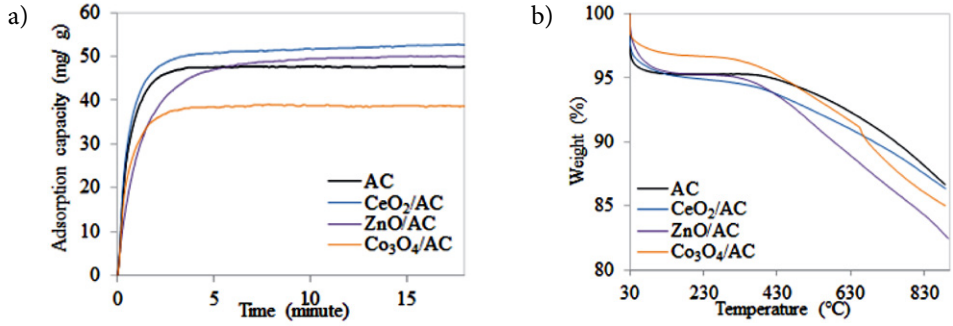

Figure 6. a) CO_2 adsorption at 30 °C and b) desorption process until 400 °C.

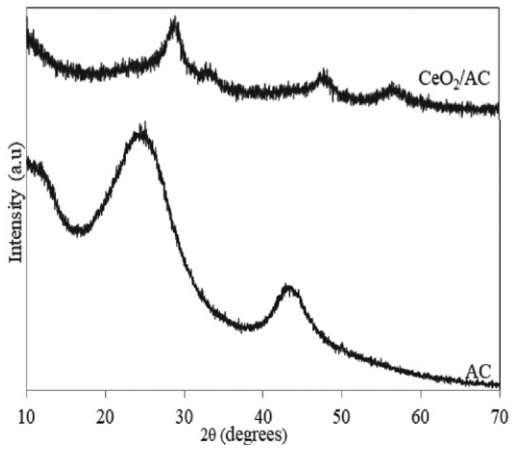

Figure 7. XRD diffractograms.

slightly enlarged pore structure. The SEM image supports the prediction from the textural properties with a possible ability of the CeO_2 to enter the pores of AC and deposit on the AC surfaces.

3. 3. Recyclability Test

Five cycles of CO_2 adsorption-desorption was conducted to optimize the performance for CeO_2/AC at different adsorption temperature of 30 and 50 °C (Figure 9). It is interesting to note that the adsorption capacity is higher for the adsorption temperature of 30 °C than 50 °C. At adsorption temperature of 30 °C, the loss in adsorption capacity was only 6.53% with a decrease from first to fifth cycles is 52.50 mg CO_2/ g adsorbent to 49.07 mg CO_2/g

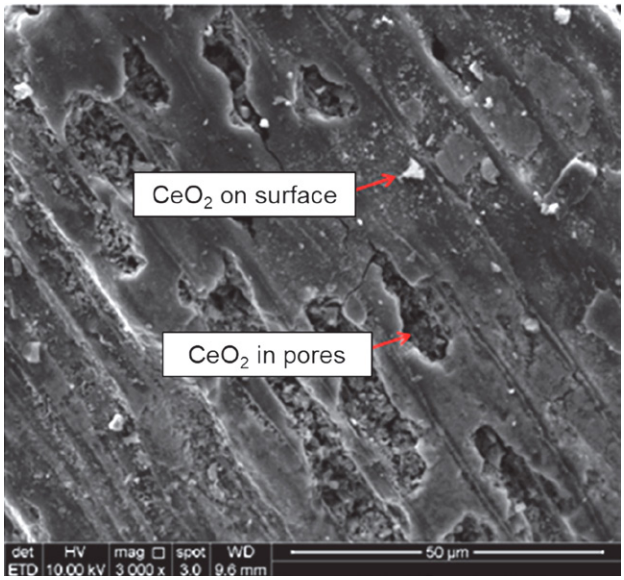

Figure 8. SEM image of CeO_2/AC.

adsorbent, respectively. At adsorption temperature of 50 °C, there was a 7.86% loss in adsorption capacity with a decrease from the first to fifth cycles is 40.56 mg CO_2/ g adsorbent to 37.37 mg CO_2/ g adsorbent, respectively. These observations may suggest that adsorption capacity decreases as the adsorption temperature increases. According to Rashidi *et al.*,[51] an exothermic process where physisorption is favored at lower temperature implies the existence of physisorption throughout the process of adsorption. Thus, at a temperature above 30 °C, the adsorbate of CO_2 has the tendency to desorb during the adsorption period reaching its equilibrium which eventually leads to lower adsorption capacity.

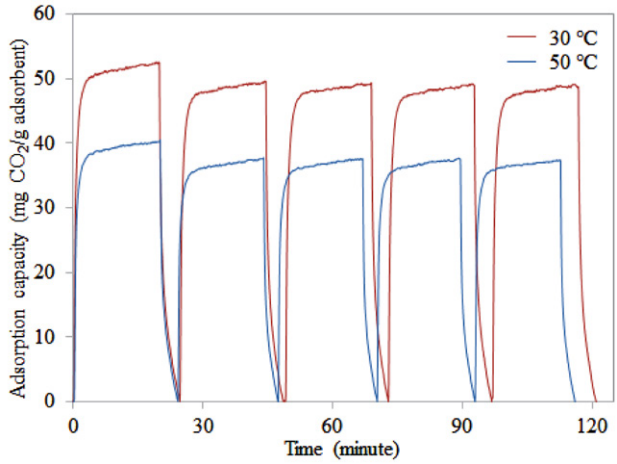

Figure 9. Five cycles of CO_2 capture at adsorption temperature of 30 and 50 °C.

3. 4. Kinetic Analysis

The CO_2 adsorption kinetics data for CeO_2/AC at different operating adsorption temperatures from the first cycle was adjusted by using two kinetic models, namely pseudo-first-order (Equation 3) and pseudo-second-order kinetic model (Equation 4).

$$\log(q_e - q_t) = \log q_e - \left(\frac{k_1}{2.303}\right) t \quad (3)$$

$$\frac{t}{q_t} = \frac{1}{k_2 q_e^2} + \left(\frac{1}{q_e}\right) t \quad (4)$$

where q_t and q_e are the adsorption capacity at any particular time t and at equilibrium, respectively, and k_1 is the pseudo-first-order kinetic constant, k_2 is the pseudo-second-order kinetic constant and ($k_2 \cdot q_e^2$) is initial adsorption rate. The kinetic linear plot using the two equations for evaluating the mechanism of the adsorption process is shown in Figure 10. The kinetic parameters are tabulated in Table 5.

The pseudo-first-order kinetic model describes the initial phase and the progress of adsorption. The value of $\log(q_e - q_t)$ were calculated from the kinetic data. The graph was plotted for $\log(q_e - q_t)$ against t based on the calculations (Figure 10 a). Next, k_1 was calculated from the slope of the plotted graph. It is clear that calculated adsorption capacity also significantly deviates from the actual adsorption capacity, which is similar to findings for this model with Rashidi *et al.*[51] and Gopal *et al.*[52] Thus, this study does not support pseudo-first-order kinetic model, in addition to the low R^2 value at 0.9178 and 0.8777 for CO_2 adsorption at 30 and 50 °C, respectively. The kinetic data obtained in this study failed to fit this model, which appears to be invalid for this work.

In the case of pseudo-second-order kinetic model, it describes the control of the chemisorption in the speed of progress. A graph was plotted for t/q_t against t as shown in Figure 10 b). Next, k_2 was calculated from the slope of the plot. Based on the Table 5, it shows high correlation coefficient values of R^2 are 0.9994 and 0.9622 for both adsorption temperatures of 30 and 50 °C, respectively, which support the adsorption capacity of CO_2 toward the CeO_2/AC. The relative error between actual and calculated adsorption capacity were comparatively lower than that of pseudo-first-order kinetic model. It has the relative error calculated for adsorption temperatures of 30 and 50 °C at 1.32 and 2.74%, respectively.

Based on these R^2 values and relative errors, the pseudo-second-order kinetic model is indeed the most suitable model for the CO_2 adsorption kinetic profiles at both adsorption temperatures of 30 and 50 °C. This suggests the CO_2 adsorption is inclined towards chemisorption in the existence of both physisorption and chemisorption. It might be the limiting step involving the exchange of electron between CeO_2 and CO_2 adsorbate resulting in the adsorption process mainly governed by monolayer adsorption referring to chemical phenomena. However, the presence of physisorption remains undeniable due to the fact that adsorbent is AC based material which may form

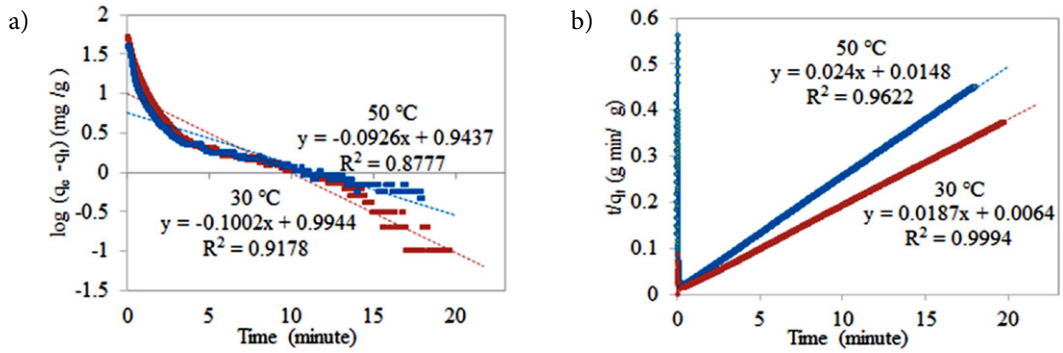

Figure 10. Kinetic plot a) pseudo-first-order kinetic model and b) pseudo-second-order kinetic model at different adsorption temperatures for CeO_2/AC.

Table 5. Kinetic parameters of CO_2 adsorption onto CeO_2/AC.

Kinetic model	Parameter	Temperature (°C) 30	50
	$q_{e(act)}$ (mg/g)	52.78	40.56
Pseudo-first order kinetic	$q_{e(cal)}$ (mg/g)	9.87	8.78
	k_1(1/min)	0.2308	0.2132
	R^2	0.9178	0.8777
	Relative error (%)	81.29	78.34
Pseudo-second-order kinetic	$q_{e(cal)}$ (mg/g)	53.47	41.67
	k_2 (g/mg min)	0.0546	0.0389
	h (mg/g min)	156.14	67.57
	R^2	0.9994	0.9622
	Relative error (%)	1.32	2.74

where $q_{e(act)}$ = actual adsorption capacity; $q_{e(cal)}$ = calculated adsorption capacity

Van der Waals forces with CO_2. This proves that AC surface reactivation with the addition of CeO_2 could enhance the adsorption capacity by chemisorption.

4. Conclusion

Various metal oxides impregnated on chemically reactivated AC were successfully synthesized. SEM images and XRD pattern confirmed that CeO_2 is highly dispersed on the AC surface. FTIR showed the characteristic peaks for the increased oxygen-containing functional group on activated carbon. All the MO/AC showed great thermal stability with high resistance toward heat up to 900 °C except for Co_3O_4/AC. The CeO_2/AC exhibits the most efficient adsorbent with an adsorption capacity of 52.78 mg/g at the equilibrium state of 10 minutes. It showed only a 6.53% loss in adsorption capacity after five cycles with adsorption temperature at 30 °C and a relatively lower desorption temperature of 160–280 °C, which requires less energy consumption. The pseudo-second-order kinetic model was best fitted compared to the pseudo-first-order kinetic model with a higher correlation coefficient. Besides, the pseudo-second-order-kinetic model yields the closest values for calculated adsorption quantity to the actual adsorption quantity. This significantly implies both physisorption and chemisorption for CeO_2/AC.

Acknowledgement

The authors are grateful to the Department of Science and Technology, Universiti Putra Malaysia Kampus Bintulu and School of Chemical Sciences, Univerisiti Sains Malaysia for the research facilities. The authors wish to thanks the Ministry of Higher Education for the financial support for grant numbers of GP-IPM-9657200, GP-IPM-9559000, 1001.PKIMIA.811333 and 1001.PKIMIA.822215.

5. References

1. National Oceanic and Atmospheric Administration (NOAA), Recent Global CO_2, https://www.esrl.noaa.gov/gmd/ccgg/trends/global.html (accessed: March 3rd, 2020)
2. N. Mimura, *P. Jpn. Acad. B Phys. Bio. Sci.* **2013,** 89(6), 281–301. **DOI:**10.2183/pjab.89.281
3. J. R. Fanchi, C. J. Fanchi, Energy in the 21st Century, Fourth Edition, World Scientific, Singapore, Singapore, **2016.** **DOI:**10.1142/10160
4. B. Metz, O. Davidson, H. D. Coninck, M. Loos, L. Meyer, IPCC special report on carbon dioxide capture and storage, Cambridge University Press, New York, United States, **2005**.
5. W. Yuan, Z. Li, A. Otto, M. Robinius, D. Stolten, *Energy Procedia.* **2017**, *114*, 650–665. **DOI:**10.1016/j.egypro.2017.03.1209
6. E. S. Kikkinides, R. T. Yang, S. H. Cho, *Ind. Eng. Chem. Res.* **1993**, *32*, 2714–2720. **DOI:**10.1021/ie00023a038
7. Q. Wang, Q. J. Luo, Z. Zhong, A. Borgna, *Energ. Environ. Sci.* **2011**, *4*(1), 42–55. **DOI:**10.1039/C0EE00064G
8. J. Gale, Y. Kaya, Greenhouse Gas Control Technologies, Pergamon, New York, United States, **2003**.
9. C. H. Yu, C. H. Huang, C. S. Tan, *Aerosol Air Qual. Res.* **2012**, *12*(5), 745–769. **DOI:**10.4209/aaqr.2012.05.0132

10. K. C. Chanapattharapol, S. Krachuamram, S. Youngme, *Micropor. Mesopor. Mat*. **2017**, *245*, 8–15. **DOI:**10.1016/j.micromeso.2017.02.072
11. A. E. Ogungbenro, D. V. Quang, K. Al-Ali, M. R. M. Abu-Zahra, *Energy Procedia*. **2017**, *114*, 2313–2321. **DOI:**10.1016/j.egypro.2017.03.1370
12. R. Kodasma, J. Fermoso, A. Sanna, *Chem. Eng. J.* **2018**, *358*, 1351–1362. **DOI:**10.1016/j.cej.2018.10.063
13. C. E. Bien, K. K. Chen, S. C. Chien, B. R. Reiner, L. C. Lin, C. R. Wade, W. S. W. Ho, *J. Am. Chem. Soc.* **2018,** *140*(40), 12662–12666. **DOI:**10.1021/jacs.8b06109
14. S. S. Shang, A. Hanif, M. Z Sun, Y. M. Tian, Y. S. Ok, I. K. M.Yud, D. C.W. Tsang, Q. F. Gue, J. Shang, *J. Hazard, Mater*. **2019,** *373*, 285–293. **DOI:**10.1016/j.jhazmat.2019.03.077
15. M. N. Abu Tahari, A. Hakim, T. S. Marliza, N. H. Mohd, M. A. Yarmo, *Mater. Sci. Forum* **2017,** *888*, 529–533. **DOI:**10.4028/www.scientific.net/MSF.888.529
16. M. A. Naeem, A. Armutlulu, Q. Imtiaz, C. R. Meller, *ChemPhysChem*. **2017,** *18*, 3280–3285. **DOI:**10.1002/cphc.201700695
17. A. Boonpoke, S. Chiarakorn, N. Laosiripojana, S. Towprayoon, *Korean J. Chem. Eng.* **2012**, *29*, 89–94. **DOI:**10.1007/s11814-011-0143-0
18. K. S. N. Kamarudin, N. Zaini, N. E. A. Khairuddin, *J. Environ. Chem. Eng.* **2018,** *6*, 549–559. **DOI:**10.1016/j.jece.2017.12.040
19. S. Lin, T. Kiga, Y. Wang, K. Nakayama, *Energy Procedia* **2011,** *4*, 356–361. **DOI:**10.1016/j.egypro.2011.01.062
20. S. C. Tian, J. G. Jiang, F. Yan, K. M. Li, X. J. Chen, V. Manovic, *Green Chem*. **2016,** *18*, 4022–4031. **DOI:**10.1039/C6GC00400H
21. S. Wongsakulphasatch, K. Sukchoknamchai, N. Suthapot, W. Praikaew, C. Chaisuk, W. Kiatkittipong, N. Laosiripojana, S. Assabumrungrat, S. *MATEC Web of Conferences* **2018,** 192, 03057. **DOI:**10.1051/matecconf/201819203057
22. A. Hakim, T. S. Marliza, M. N. Abu Tahari, W. N. R. Wan Isahak, M. R. Yusop, M. W. Mohamed Hisham, M. A. Yarmo, *Ind. Eng. Chem. Res.* **2016,** *55*(29), 7888–7897. **DOI:**10.1021/acs.iecr.5b04091
23. J. Baltrusaitis, J. Schuttlefield, E. Zeitler, V. H. Grassian, 2011. *Chem. Eng. J.* 2011, *170*, 471–481. **DOI:**10.1016/j.cej.2010.12.041
24. K. Yoshikawa, H. Sato, M. Kaneeda, J. N. Kondo, *J. CO_2 Util.* **2014,** *8*, 34–38. **DOI:**10.1016/j.jcou.2014.10.001
25. Y. M. Wang, R. Kováčik, B. Meyer, K. Kotsis, D. Stodt, V. Staemmler, H. S. Qiu, F. Traeger, D. Langenberg, M. Muhler, C. Wöll, *Angew. Chem. Int. Edit*. **2007,** *46*, 5624–5627. **DOI:**10.1002/anie.200700564
26. A. Hakim, M. N. Abu Tahari, T. S. Marliza, W. N. R. Wan Isahak, M. R. Yusop, M. W. M. Hisham, M. A. Yarmo, *J. Teknol. (Sci. Eng.)*. **2015,** 77(33), 75–84. **DOI:**10.11113/jt.v77.7010
27. A. Hakim, W. N. R. Wan Isahak, M. N. Abu Tahari, M. R. Yusop, M. H. Mohamed Wahab, M. A. Yarmo, *Adv. Mat. Res.* **2015,** *1087*, 45–49. **DOI:**10.4028/www.scientific.net/AMR.1087.45
28. Y. J. Heo, S. J. Park, *Sci. Rep.* **2017,** *5653*, 1–9.
29. W. N. R. Wan Isahak, Z. A. Che Ramli, A. Z. Lahuri, M. R. Yusop, M. H. Mohamed Wahab, M. A. Yarmo, *Adv. Mat. Res.* **2015,** *1087*, 111–115. **DOI:**10.4028/www.scientific.net/AMR.1087.111
30. C. Slotowski, S. Marre, P. Dagault, O, Babot, T. Toupance, C. Aymonier, *J. CO_2 Uti.*, **2017**, *20*, 52–58. **DOI:**10.1016/j.jcou.2017.03.023
31. A. Hakim, M. A. Yarmo, T. S. Marliza, M. N. A. Tahari, W. Z. Samad, M. R. Yusop,M. W. M. Hisham, N. Dzakaria, *Malaysian J. Anal. Sci.* **2016**, *20(6)*, 1286–1298. **DOI:**10.4028/www.scientific.net/MSF.888.485
32. T. S. Marliza, M. A. Yarmo, A. Hakim, M. N. A. Tahari, Y. H. Taufiq-Yap, *Mater. Sci. Forum*, **2017**, *888*, 485–490.
33. T. S. Marliza, M. A. Yarmo, A. Hakim, M. N. A. Tahari, M. W. M. Hisham, Y. H. Taufiq-Yap, *AIP.* **2017,** *20008*, 1–8.
34. Z. Ghazali, N. H. Hassan, M. A. Yarmo, L. P. Teh, R. Othaman, *Sains Malays.* **2019**, *48(5)*, 1025–1033. **DOI:**10.17576/jsm-2019-4805-11
35. N. Z. Zulkurnai, U. F. Md. Ali, N. Ibrahim, N. S. Abdul Manan, *E3S Web Conf.* **2018**, *34*, 02030. **DOI:**10.1051/e3sconf/20183402030
36. S. Ge, Z. Liu, Y. Furuta, W. Peng, *Saudi J. Biol. Sci*. **2017**, *24*(6), 1370–1374. **DOI:**10.1016/j.sjbs.2016.12.016
37. G. Zhang, J. Qu, H. Liu, A. T. Cooper, R. Wu, *Chemosphere* **2007,** *68*(6), 1058–1066. **DOI:**10.1016/j.chemosphere.2007.01.081
38. G. Zhang, Y. Sun, P. Zhao, Y. Xu, A. Su, J. Qu, *J. CO_2 Util.* **2017,** *20*, 129–140. **DOI:**10.1016/j.jcou.2017.05.013
39. H. Zhao, F. Wang, Y. Ning, B. Zhao, F. Yin, Y. Lai, K. Hu, *Sci. Rep*. **2013,** *3*, 1511. **DOI:**10.1038/srep01511
40. G. H. Hara Priya, N. Sunganya, V. Jaisankar, *Int. J. Adv. Chem. Sci. Appl.* **2015,** *3*, 6–14.
41. K. S. W. Sing, D. H. Everett, R. A. W. Haul, L. Moscou, R. A. Pierotti, J. Rouquerol, *Pure & Appl. Chem.* **1985,** *57*(4), 603–619.
42. J. B. Condon, Surface Area and Porosity Determinations by Physisorption: Measurements and Theory, first ed., Oxford, United Kingdom, Elsevier B. V., **2006.**
43. G. A. El-Shobaky, A. S. Ahmad, A. N. Al-Noaimi, H. G. El-Shobaky, *J. Therm. Anal.* **1996,** *46*(6), 1801–1808. **DOI:**10.1007/BF01980784
44. P. Ferstl, S. Mehl, M. A. Arman, M. Schuler, A. Toghan, B. Laszlo, J. Knudsen, *J. Phys. Chem. C* **2015,** *119*(29), 16688–16699. **DOI:**10.1021/acs.jpcc.5b04145
45. V. Savin, V. Sobolev, Z. Eremenko, Z. Grigor'eva, *J. Anal. Chem.-USSR.* **1985,** *59*(3), 571–575.
46. H. Madzaki, W. A. W. A. K. Ghani, S. Y. Thomas Choong, U. Rashid, N. Muda, *J. Kejuruteraan.* **2018,** *30(1)*, 31–38. **DOI:**10.17576/jkukm-2018-30(1)-05
47. I. Senturk, M. Alzein, *Acta Chim. Slov.* **2020,** 67, 1–15. **DOI:**10.17344/acsi.2019.5195
48. A. R. Hidayu, N. Muda, *Procedia Eng.* **2016,** 148, 106–113. **DOI:**10.1016/j.proeng.2016.06.463
49. M. G. Plaza, A. S. Gonzalez, C. Pevida, J. J. Pis, F. Rubiera, *Appl. Energy*. **2012,** 99, 272–279. **DOI:**10.1016/j.apenergy.2012.05.028

50. H. Qin, H. Chen, X. Zhang, G. Yang, Y. Feng, *J. Chem. Technol. Biot.* **2014,** *89*(9), 1402–1409. **DOI:**10.1002/jctb.4222
51. N. A. Rashidi, S. Yusup, B. H. Hameed, *Energy.* **2013**, *61*, 440–446. **DOI:**10.1016/j.energy.2013.08.050
52. K. Gopal, N. I. Mohd, M. Raoov, F. B. M. Suah, N. Yahaya, N. N. M. Zain, *RSC. Adv*. **2019**, *9*, 36915–36930. **DOI:**10.1039/C9RA07151B

Povzetek

Za določitev učinkovitosti zajemanja (adsorpcije) CO_2 in analizo adsorpcije z raznimi kinetičnimi modeli so bili sintetizirani različni kovinski oksidi (CeO_2, ZnO in Co_3O_4), ki smo jih impregnirali na aktivnem oglju (AC). Šaržne kinetične študije so pokazale, da je CeO_2/AC najučinkovitejši adsorbent, kjer je bil čas do vzpostavitve ravnotežja le 10 minut in adsorpcijska zmogljivost 52,68 mg/g. Adsorpcija CO_2 je optimalna pri temperaturi 30° C z le 6,53% izgubo adsorpcijske zmogljivosti po 5 ciklih adsorpcije in desorpcije CO_2. CeO_2 na AC je bil karakteriziran z rentgensko difrakcijo in vrstično elektronsko mikroskopijo, ki kažeta dobro razporejene delce CeO_2 na AC površinah. Kinetika adsorpcije CO_2 pri 30 ° C se najbolje ujema s kinetičnim modelom psevdo drugega reda z R^2 = 0,9994 in relativno napako med izračunano in eksperimentalno adsorpcijsko zmogljivostjo le 1,32%. Za izboljšanje adsorpcijske sposobnosti je odgovorna kemisorpcija. Dodatek CeO_2 na AC je povečal adsorpcijsko sposobnost z zagotavljanjem aktivnih mest, ki privlačijo CO_2.